

# Spectroscopic Characterization of Mononitrosyl Complexes in Heme–Nonheme Diiron Centers within the Myoglobin Scaffold (Fe<sub>B</sub>Mbs): Relevance to Denitrifying NO Reductase

Takahiro Hayashi,<sup>†</sup> Kyle D. Miner,<sup>‡</sup> Natasha Yeung,<sup>‡</sup> Ying-Wu Lin,<sup>‡</sup> Yi Lu,<sup>‡</sup> and Pierre Moënne-Loccoz<sup>\*,†</sup>

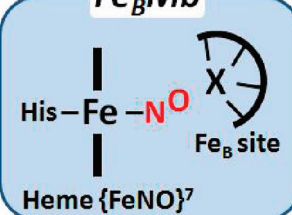
<sup>†</sup>Division of Environmental and Biomolecular Systems, Oregon Health and Science University, Beaverton, Oregon 97006, United States

<sup>‡</sup>Department of Chemistry, University of Illinois, Urbana, Illinois 61801, United States

**S** Supporting Information

**ABSTRACT:** Denitrifying NO reductases are evolutionarily related to the superfamily of heme-copper terminal oxidases. These transmembrane protein complexes utilize a heme–nonheme diiron center to reduce two NO molecules to N<sub>2</sub>O. To understand this reaction, the diiron site has been modeled using sperm whale myoglobin as a scaffold and mutating distal residues Leu-29 and Phe-43 to histidines and Val-68 to a glutamic acid to create a nonheme Fe<sub>B</sub> site. The impact of incorporation of metal ions at this engineered site on the reaction of the ferrous heme with one NO was examined by

UV–vis absorption, EPR, resonance Raman, and FTIR spectroscopies. UV–vis absorption and resonance Raman spectra demonstrate that the first NO molecule binds to the ferrous heme, but while the apoproteins and Cu<sup>I</sup>- or Zn<sup>II</sup>-loaded proteins show characteristic EPR signatures of *S* = 1/2 six-coordinate heme {FeNO}<sup>7</sup> species that can be observed at liquid nitrogen temperature, the Fe<sup>II</sup>-loaded proteins are EPR silent at ≥ 30 K. Vibrational modes from the heme [Fe–N–O] unit are identified in the RR and FTIR spectra using <sup>15</sup>NO and <sup>15</sup>N<sup>18</sup>O. The apo and Cu<sup>I</sup>-bound proteins exhibit *ν*(FeNO) and *ν*(NO) that are only marginally distinct from those reported for native myoglobin. However, binding of Fe<sup>II</sup> at the Fe<sub>B</sub> site shifts the heme *ν*(FeNO) by 17 cm<sup>−1</sup> and the *ν*(NO) by −50 cm<sup>−1</sup> to 1549 cm<sup>−1</sup>. This low *ν*(NO) is without precedent for a six-coordinate heme {FeNO}<sup>7</sup> species and suggests that the NO group adopts a strong nitroxyl character stabilized by electrostatic interaction with the nearby nonheme Fe<sup>II</sup>. Detection of a similarly low *ν*(NO) in the Zn<sup>II</sup>-loaded protein supports this interpretation.

<i>Fe<sub>B</sub>Mb</i>	
	
X	<i>ν</i> (NO) / cm <sup>−1</sup>
Fe <sup>2+</sup>	1549 <b>Low!</b>
Zn <sup>2+</sup>	1550/1577
Cu <sup>+</sup>	1601
apo	1601

Nitric oxide reductases (NORs) from denitrifying bacteria catalyze the two-electron reduction of nitric oxide (NO) to nitrous oxide (N<sub>2</sub>O) as a part of the denitrification process that converts nitrite (NO<sub>2</sub><sup>−</sup>) and nitrate (NO<sub>3</sub><sup>−</sup>) to dinitrogen gas (N<sub>2</sub>).<sup>1–3</sup> This catalytic reduction of toxic NO to the relatively unreactive N<sub>2</sub>O gas has been shown to provide some pathogenic bacteria resistance to the mammalian immune response.<sup>4,5</sup> NORs are integral membrane proteins and are evolutionally related to the heme-copper oxidases (HCOs). The first crystal structure of a cytochrome *c*-dependent NOR (cNOR) was recently determined to a resolution of 2.7 Å (Figure 1A).<sup>6</sup> As expected from sequence alignments and homology models, the NorB catalytic subunit of cNOR exhibits strong structural homology to subunit I of HCOs with 12 central transmembrane helices and six conserved histidine residues responsible for anchoring the low-spin heme and binuclear active site, i.e., the heme *b*<sub>3</sub>–nonheme Fe<sub>B</sub> center of cNOR and heme *a*<sub>3</sub>–Cu<sub>B</sub> centers of HCOs.

Despite differences in the active site metal composition, NO and O<sub>2</sub> reductase activities are catalyzed by both families of enzymes, with NORs showing limited oxidase activity and several HCOs (i.e., *ba*<sub>3</sub>, *bo*<sub>3</sub>, and *cbb*<sub>3</sub>) being capable of reducing NO to

N<sub>2</sub>O.<sup>7,8</sup> Previously, we investigated the structure of heme-nitrosyl {FeNO}<sup>7</sup> complexes in cytochrome *ba*<sub>3</sub> and *bo*<sub>3</sub> and concluded that the mechanism of NO reduction in HCOs could accommodate differences in Cu<sub>B</sub> reactivity toward NO.<sup>9,10</sup> This conclusion suggested that coordination of a second NO to Cu<sub>B</sub> to form a [heme-NO·Cu<sub>B</sub>-NO] trans-dinitrosyl complex, as proposed by Varotsis and co-workers,<sup>11,12</sup> is not an essential step in the NO reduction reaction in HCOs. A theoretical study by Siegbahn and co-workers predicts that after binding of a first NO to the heme iron(II), a second NO can directly attack the heme-nitrosyl complex to form a heme iron(III)-hyponitrite dianion complex stabilized by electrostatic interaction with the Cu<sub>B</sub><sup>II</sup> sites.<sup>13</sup> A similar route of NO reduction can be envisioned at the heme–nonheme diiron site of NOR.<sup>14</sup>

We now direct our work to active site models of NORs. Specifically, Lu and co-workers have engineered myoglobin to mimic the heme–nonheme diiron site of NORs by constructing an Fe<sub>B</sub> site in the distal heme pocket with three histidines and one

**Received:** March 18, 2011

**Revised:** May 16, 2011

**Published:** June 02, 2011

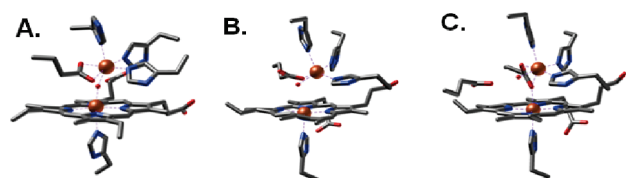


**Figure 1.** Heme–nonheme diiron centers of oxidized cNOR from *Pseudomonas aeruginosa* [Protein Data Bank (PDB) entry 3O0R] (A), reduced Fe<sup>II</sup>-Fe<sub>B</sub>Mb1 (PDB entry 3K9Z) (B), and reduced Fe<sup>II</sup>-Fe<sub>B</sub>Mb2 (PDB entry 3M39) (C).

glutamate residue (L29H, F43H, H64, and V68E, hereafter called Fe<sub>B</sub>Mb1). In a second-generation construct, a glutamate side chain at the periphery of the two metal ions' open coordination sites has been included in the model (L29H, F43H, H64, V68E, and I107E, hereafter called Fe<sub>B</sub>Mb2). The crystal structures of reduced Fe<sub>B</sub>Mb1 and Fe<sub>B</sub>Mb2 loaded with Fe<sup>II</sup> (Fe<sup>II</sup>-Fe<sub>B</sub>Mb1 and Fe<sup>II</sup>-Fe<sub>B</sub>Mb2, respectively) confirm coordination of the nonheme iron(II) by three histidines, one glutamate, and a solvent molecule, as observed for the Fe<sub>B</sub> center of cNOR (Figure 1).<sup>15,16</sup> Although the NO reductase activity of these models appears to be limited, they represent an excellent opportunity for the structural analysis of the initial interactions of NO with the diiron site of NORs in the absence of other redox-active chromophores and without the practical difficulties associated with membrane proteins. Here, we report that the reaction of reduced Fe<sup>II</sup>-Fe<sub>B</sub>Mb1 and Fe<sup>II</sup>-Fe<sub>B</sub>Mb2 with 1 equiv of NO produces stable six-coordinate low-spin (6cLS) heme {FeNO}<sup>7</sup> complexes with exceptionally low  $\nu(\text{NO})$  stretching frequencies. Spectroscopic data with Zn<sup>II</sup> and Cu<sup>I</sup> substitutions at the Fe<sub>B</sub> site support the assignment of this low  $\nu(\text{NO})$  to stabilization of a heme Fe(III)-NO<sup>-</sup> electronic configuration by electrostatic interaction with Fe<sub>B</sub><sup>II</sup>. The relevance of this [heme-NO·Fe<sub>B</sub>] complex to the mechanism of NO reduction at the heme–nonheme center of NORs is discussed.

## MATERIALS AND METHODS

**Protein Preparations and Metal Titrations.** The expression and purification of Fe<sub>B</sub>Mb1 (swMb L29H/F43H/V68E) and Fe<sub>B</sub>Mb2 (swMb L29H/F43H/V68E/I107E) were performed as previously described.<sup>15,16</sup> All protein concentrations were calculated on the basis of a 406 nm extinction coefficient,  $\epsilon_{406}$ , of 175 mM<sup>-1</sup> cm<sup>-1</sup> in the oxidized proteins. Apo-Fe<sub>B</sub>Mb solutions at 1 mM were brought into a glovebox containing <1 ppm of O<sub>2</sub> (Omnilab System, Vacuum Atmospheres Co.). The proteins were reduced by addition of ~5 mM dithionite followed by removal of excess reduction agents with desalting spin columns (Zebra, Pierce). Additions of Zn<sup>II</sup> and Cu<sup>II</sup> were performed prior to the reduction in 50 mM Bis-Tris (pH 7.0) using Zn<sup>II</sup>SO<sub>4</sub> and Cu<sup>II</sup>SO<sub>4</sub> salts, while addition of Fe<sup>II</sup> was performed after the reduction in the same buffer using Fe<sup>II</sup>Cl<sub>2</sub>. Fresh Fe<sup>II</sup>, Zn<sup>II</sup>, and Cu<sup>II</sup> solutions were prepared each time by dissolving Fe<sup>II</sup>Cl<sub>2</sub>, Zn<sup>II</sup>SO<sub>4</sub>, and Cu<sup>II</sup>SO<sub>4</sub>, respectively, in 0.01 M HCl or doubly distilled water. Typically, 3  $\mu$ L of a metal solution containing 1.3–2 equiv of metal was added to 100  $\mu$ L of a 1 mM protein solution at a rate of 0.5  $\mu$ L/min with gentle stirring. After metal had been added, the protein solution was incubated at room temperature for 20 min and incorporation of the metal ion was confirmed by UV–vis spectroscopy using a Cary 50 spectrophotometer (Varian). If required, the samples were concentrated

with a microcon filtering device (10 kDa cutoff, Amicon ultra, Millipore).

**Preparation of NO Adducts.** Stoichiometric additions of NO to fully reduced proteins were made using NO-saturated stock solutions (<sup>14</sup>NO purchased from Airgas and <sup>15</sup>NO and <sup>15</sup>N<sup>18</sup>O from Aldrich, treated with a 1 M KOH solution) tested by titration with deoxymyoglobin (Sigma). Alternatively, diethylamine NONOate (Cayman Chemical, Ann Arbor, MI) was used as a NO donor by preparing a stock solution in 0.01 M NaOH on the basis of an  $\epsilon_{250}$  of 6500 M<sup>-1</sup> cm<sup>-1</sup>. Additions of NO were made either in anaerobic UV–vis cuvettes or in Eppendorf tubes followed by immediate transfer of the sample solutions to EPR tubes, Raman capillaries, or FTIR cells. The presence of the NO complexes was confirmed by obtaining UV–vis absorption spectra of all samples directly in EPR tubes, Raman capillaries, or FTIR cells. CO/NO mixed-gas experiments were conducted as previously described with slight modifications.<sup>10</sup> The sample headspace was thoroughly exchanged with pure CO gas to reach saturation (Airgas) and incubated for a few minutes at room temperature. Immediately after addition of 1.0 equiv of NO as NONOate, the protein solution was transferred to an FTIR cell with a 15  $\mu$ m Teflon spacer.

**Molecular Spectroscopy.** UV–vis absorption spectra were recorded on a Varian Cary 50 instrument. EPR spectra were obtained with a Bruker E500 X-band EPR spectrometer equipped with a superX microwave bridge and a dual-mode cavity with a helium flow cryostat (ESR900, Oxford Instrument, Inc.) for measurements at 5–40 K and a super HiQ cavity resonator (ESR4122, Bruker) and a liquid nitrogen Dewar for measurements above 90 K. Quantitation of the EPR signals was performed under nonsaturating conditions by double integration and comparison with Cu<sup>II</sup>-EDTA standards. RR spectra were recorded using a custom McPherson 2061/207 spectrograph (set at 0.67 m with variable gratings) equipped with a liquid N<sub>2</sub>-cooled CCD detector (LN-1100PB, Princeton Instruments). The 413 nm excitation laser was derived from a Kr laser (Innova 302C, Coherent) and the 442 nm line from a helium–cadmium laser (Liconix, Santa Clara, CA). A Kaiser Optical supernotch filter or a long-pass filter (RazorEdge, Semrock) was used to attenuate Rayleigh scattering. RR spectra were recorded at room temperature in a 90° scattering geometry on samples mounted on a reciprocating translation stage. To assess the photosensitivity of the NO adduct, we compared rapid acquisitions with minimal laser power and continuous sample spinning with longer data acquisitions on static samples. Frequencies were calibrated relative to indene and aspirin standards and are accurate to  $\pm 1$  cm<sup>-1</sup>. Polarization conditions were optimized using CCl<sub>4</sub> and indene. The integrity of the RR samples was confirmed by direct monitoring of their UV–vis absorption spectra in Raman capillaries before and after laser exposure. Typical enzyme concentrations ranged from 10  $\mu$ M for UV–vis measurements in cuvettes to 100  $\mu$ M for EPR and RR samples.

FTIR photolysis experiments were conducted as described previously.<sup>9,10</sup> Approximately 15  $\mu$ L of a 1 mM protein solution was loaded in an FTIR cell with a 15  $\mu$ m path length. The FTIR cell was mounted to a sample rod and flash-frozen in liquid N<sub>2</sub>, prior to insertion in a precooled closed-cycle cryogenic system (Omniplex, Advanced Research System). The sample was kept inside the sample compartment of the FTIR or UV–vis instrument in the dark while the sample was cooled to 10 K. FTIR spectra were recorded on a Bruker Tensor 27 instrument equipped with a liquid N<sub>2</sub>-cooled MCT detector. Sets of 1000-scan

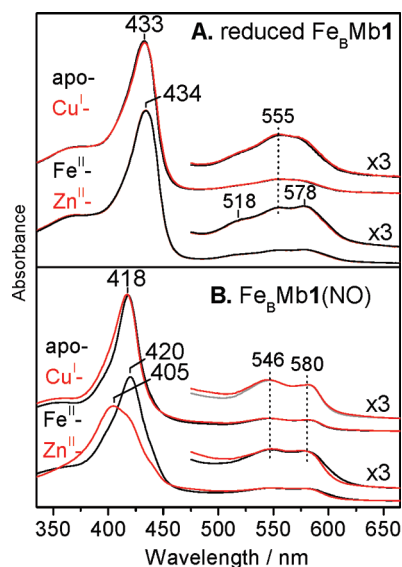


**Figure 2.** Room-temperature UV–vis absorption spectra of reduced apo-, Fe<sup>II</sup>-, Zn<sup>II</sup>-, and Cu<sup>I</sup>-Fe<sub>B</sub>Mb1 (A) and after addition of 1 equiv of NO (B).

accumulations were acquired at 4 cm<sup>-1</sup> resolution. Photolysis of the nitrosyl complexes was performed by continuous illumination of the sample directly in the FTIR sample chamber using a 300 W arc lamp after filtering heat and NIR emissions. The same illumination procedure was used to follow the dissociation process by UV–vis spectroscopy with the Cary 50 spectrophotometer. The temperature dependence of the rebinding process was monitored by increasing the sample temperature incrementally by 10 K and collecting UV–vis absorption spectra after an incubation period of 10 min. This approach provides a qualitative means of comparing rebinding temperatures between distinct photolabile species.

## RESULTS

**Characterization of Apo-, Fe<sup>II</sup>-, Zn<sup>II</sup>-, and Cu<sup>I</sup>-Fe<sub>B</sub>Mbs.** Addition of Fe<sup>II</sup> and Zn<sup>II</sup> to dithionite-reduced Fe<sub>B</sub>Mb1 results in small changes in Soret and  $\alpha/\beta$  absorption features from the ferrous heme prosthetic group compared to the apoprotein. Specifically, the Soret band observed at 433 nm in the apoprotein undergoes a red shift to 434 nm, and prominent shoulders appear at 518 and 578 nm in the visible region when divalent metal ions are bound at the Fe<sub>B</sub> site (Figure 2A).<sup>15</sup> In contrast, the presence of Cu<sup>I</sup> does not modify the UV–vis spectrum of reduced Fe<sub>B</sub>Mb1, although FTIR experiments confirm full occupancy of the Fe<sub>B</sub> site by Cu<sup>I</sup> (see below). Nearly identical observations are made by UV–vis absorption characterization of reduced apo-, Fe<sup>II</sup>-, Zn<sup>II</sup>-, and Cu<sup>I</sup>-Fe<sub>B</sub>Mb2 (Figure S1 of the Supporting Information).

The coordination number and spin state of the heme iron(II) in reduced apo-, Fe<sup>II</sup>-, Zn<sup>II</sup>-, and Cu<sup>I</sup>-Fe<sub>B</sub>Mb1 are revealed by the frequency of porphyrin vibrational modes in RR spectra obtained with Soret excitation. The reduced apo-, Fe<sup>II</sup>-, Zn<sup>II</sup>-, and Cu<sup>I</sup>-Fe<sub>B</sub>Mb1 proteins exhibit  $\nu_4$ ,  $\nu_3$ ,  $\nu_2$ , and  $\nu_{10}$  modes at 1354, 1471, 1562, and 1614 cm<sup>-1</sup>, respectively (Figure 3A). These RR frequencies are characteristic of five-coordinate high-spin (5cHS) heme iron(II). With a 442 nm excitation, the low-frequency region of the RR spectra of the reduced proteins

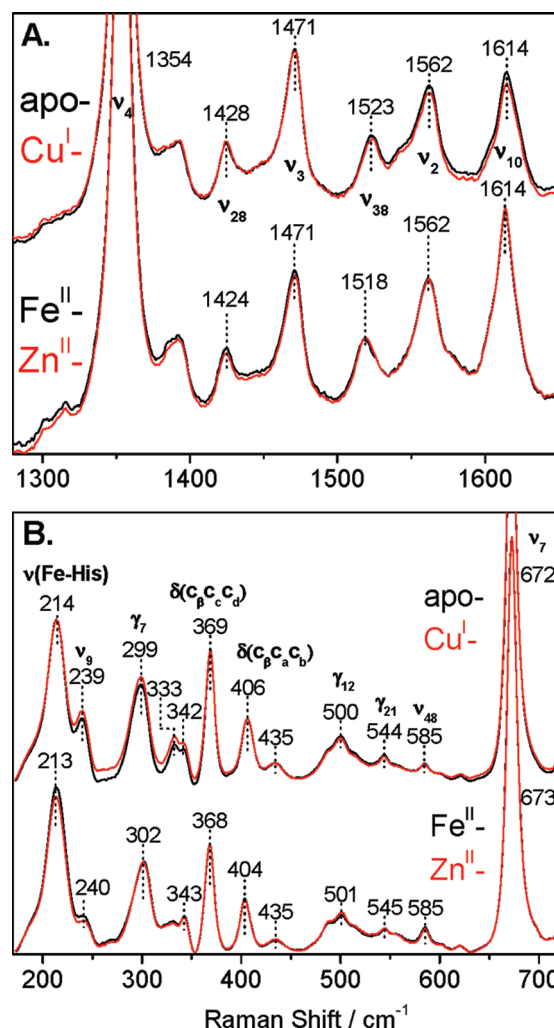


**Figure 3.** Room-temperature RR spectra of reduced apo-, Fe<sup>II</sup>-, Zn<sup>II</sup>-, and Cu<sup>I</sup>-Fe<sub>B</sub>Mb1. The high-frequency RR spectra were obtained with a 413 nm excitation (A), and low-frequency RR spectra were obtained with a 442 nm excitation (B).

exhibits an intense band between 213 and 214 cm<sup>-1</sup> that is assigned to an Fe–His stretching vibration,  $\nu(\text{Fe–N}_{\text{His}})$ , from a heme iron(II) bound to a neutral proximal histidine (Figure 3B). These  $\nu(\text{Fe–N}_{\text{His}})$  values are similar to those reported for wild-type swMb and Cu<sub>B</sub>Mb with or without Cu<sup>I</sup> bound.<sup>17–19</sup> Thus, the proximal Fe–His bond strength is not significantly affected by the distal substitutions and metal addition as expected from the crystal structure data reported for these engineered proteins.<sup>15,16</sup> As with the UV–vis data, a fine examination of the RR spectra reveals a closer match between the spectra of apo- and Cu<sup>I</sup>-Fe<sub>B</sub>Mb1 on one hand and those of Fe<sup>II</sup>- and Zn<sup>II</sup>-Fe<sub>B</sub>Mb1 on the other. Virtually identical RR spectra and  $\nu(\text{Fe–N}_{\text{His}})$  frequencies are observed with reduced apo-, Fe<sup>II</sup>-, Zn<sup>II</sup>-, and Cu<sup>I</sup>-Fe<sub>B</sub>Mb2 (Figure S2 of the Supporting Information).

**Reaction of Fe<sub>B</sub>Mbs with 1 equiv of NO.** Addition of up to 1 equiv of NO to reduced apo-, Fe<sup>II</sup>-, or Cu<sup>I</sup>-Fe<sub>B</sub>Mb1 results in blue shifts of Soret absorptions, from ~434 to ~420 nm, and the appearance of better resolved  $\alpha/\beta$  bands at 546 and 580 nm (Figure 2B). These UV–vis absorption features are consistent with the formation of six-coordinate low-spin (6cLS) heme-NO complexes and are very similar to those of the {FeNO}<sup>7</sup> complex



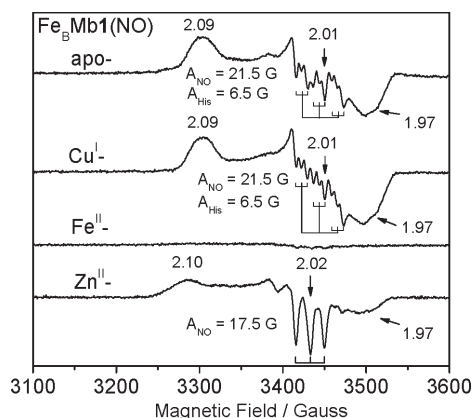


**Figure 4.** EPR spectra of apo-, Cu<sup>I</sup>-, Fe<sup>II</sup>-, and Zn<sup>II</sup>-Fe<sub>B</sub>Mb1(NO) at 30 K. Conditions: protein concentration, 100 μM; microwave frequency, 9.66 GHz; microwave power, 0.25 mW; modulation frequency, 100 kHz; modulation amplitude, 4.0 G.

formed in reduced wild-type swMb and Cu<sub>B</sub>Mb upon exposure to excess NO.<sup>19,20</sup> The nearly complete conversion of the UV–vis spectra of reduced Fe<sub>B</sub>Mb1 upon stoichiometric addition of NO suggests that the heme iron(II) has a high affinity for NO and easily outcompetes Fe<sup>II</sup> and Cu<sup>I</sup> bound at the Fe<sub>B</sub> site for NO binding. The reaction of Zn<sup>II</sup>-Fe<sub>B</sub>Mb1 with 1 equiv of NO generates a mixture of species as indicated by the presence of pronounced shoulders in the Soret absorption region (Figure 2B). The Soret band at 405 nm suggests the formation of 5cLS heme {FeNO}<sup>7</sup> species, an interpretation confirmed by the EPR analysis of these samples (see below).

Additions of 1 equiv of NO to reduced apo-, Fe<sup>II</sup>-, Cu<sup>I</sup>-, or Zn<sup>II</sup>-Fe<sub>B</sub>Mb2 produce UV–vis spectra nearly identical to those observed with Fe<sub>B</sub>Mb1, except for the Zn<sup>II</sup>-Fe<sub>B</sub>Mb2 protein, which shows a significantly smaller amount of formation of the 5cLS heme-NO complex, and consequently, a greater content of 6cLS {FeNO}<sup>7</sup> species than in Zn<sup>II</sup>-Fe<sub>B</sub>Mb1(NO) (Figure S3 of the Supporting Information). Varying conditions such as protein concentrations and the peak concentration of free NO resulted in small variations in 5cLS versus 6cLS {FeNO}<sup>7</sup> species population ratios, but we were unable to identify conditions that prevent the formation of heme coordination mixtures in the Zn<sup>II</sup>-loaded proteins.

As previously reported, the EPR spectrum of apo-Fe<sub>B</sub>Mb1(NO) is characteristic of an  $S = 1/2$  6cLS {FeNO}<sup>7</sup> species with  $g$  values centered around 2 (2.09, 2.01, and 1.97) and a clear nine-line <sup>14</sup>N hyperfine structure originating from the nitrosyl and histidine axial ligands ( $A_{\text{NO}} = 21.5$  G, and  $A_{\text{His}} = 6.5$  G) (Figure 4).<sup>16</sup> Cu<sup>I</sup>-Fe<sub>B</sub>Mb1(NO) exhibits an equivalent  $S = 1/2$  EPR signal with nine-line splitting at the center resonance ( $A_{\text{NO}} = 21.5$  G, and  $A_{\text{His}} = 6.5$  G). In contrast, this signal is not observed in the EPR spectrum of Fe<sup>II</sup>-Fe<sub>B</sub>Mb1(NO), which shows only a very weak signal centered at  $g \sim 2$  with three-line <sup>14</sup>N hyperfine structure ( $A_{\text{NO}} = 16.5$  G), typically assigned to 5cLS heme Fe<sup>II</sup>-NO species. EPR signal quantification using Cu<sup>II</sup>-EDTA standards suggests that this  $g \sim 2$  signal represents less than 5% of the Fe<sup>II</sup>-Fe<sub>B</sub>Mb1(NO) complex. Thus, the majority of the heme-nitrosyl species in Fe<sup>II</sup>-Fe<sub>B</sub>Mb1(NO) cannot be detected by EPR at  $\geq 30$  K (Figure 4). As expected from the UV–vis data, the EPR spectrum of Zn<sup>II</sup>-Fe<sub>B</sub>Mb1(NO) shows a superposition of two signals centered at  $g \sim 2$ , one exhibiting a sharp three-line <sup>14</sup>N hyperfine structure ( $A_{\text{NO}} = 17.5$  G)

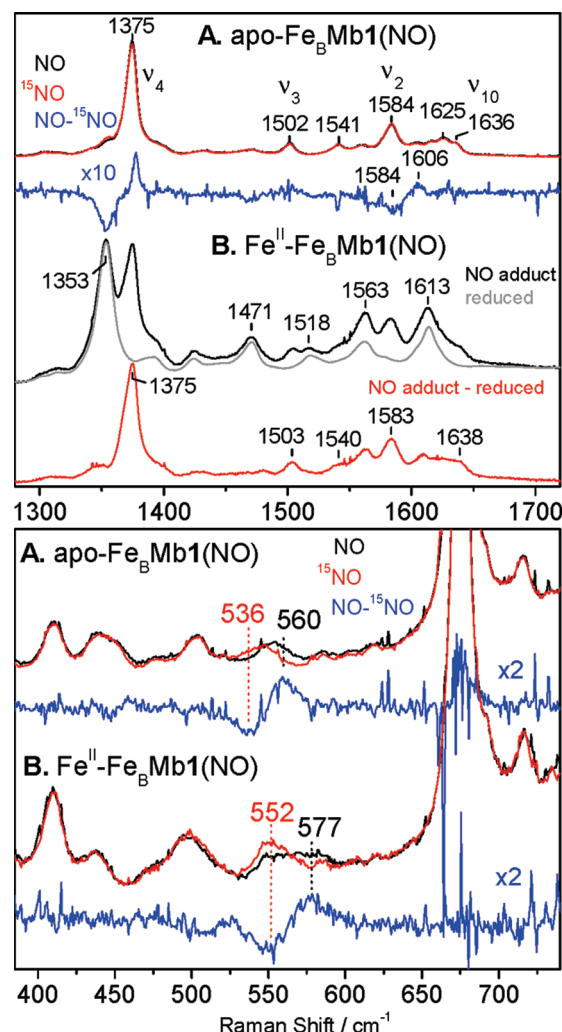


**Figure 5.** High- and low-frequency RR spectra of apo-Fe<sub>B</sub>Mb1(NO) (A) and Fe<sup>II</sup>-Fe<sub>B</sub>Mb1(NO) (B) obtained with a 413 nm excitation at room temperature.

characteristic of 5cLS heme {FeNO}<sup>7</sup> species and another with more rhombic EPR resonances suggestive of 6cLS heme {FeNO}<sup>7</sup> species. This latter species can be trapped as a photo-dissociated species at cryogenic temperatures for the isolation of its EPR components from those of the photostable 5cLS heme {FeNO}<sup>7</sup> species (Figure S4 of the Supporting Information). This coexistence of three-line and nine-line species is reminiscent of *ba*<sub>3</sub>(NO) and hemoglobin(NO) in the presence of allosteric effectors.<sup>9,21</sup> Similar EPR spectra were obtained for apo-, Fe<sup>II</sup>-, Zn<sup>II</sup>-, and Cu<sup>I</sup>-Fe<sub>B</sub>Mb2(NO). As previously suggested by the UV–vis analysis, Zn<sup>II</sup>-Fe<sub>B</sub>Mb2(NO) retains a greater content of 6cLS heme {FeNO}<sup>7</sup> species than Zn<sup>II</sup>-Fe<sub>B</sub>Mb1(NO) (Figure S4 of the Supporting Information).

EPR measurements taken below 30 K reveal new  $g = 6.2$  and  $6.1$  resonances in Fe<sup>II</sup>-Fe<sub>B</sub>Mb1(NO) and Fe<sup>II</sup>-Fe<sub>B</sub>Mb2(NO) that are absent from the EPR spectra of their apo-, Cu<sup>I</sup>-, and Zn<sup>II</sup>-Fe<sub>B</sub>Mb(NO) counterparts (Figure S5 of the Supporting Information). These nonsaturating signals are likely to reflect the  $S = 3/2$  or  $5/2$  overall spin expected from exchange coupling between the  $S = 1/2$  heme 6cLS {FeNO}<sup>7</sup> and  $S = 2$  nonheme Fe<sup>II</sup> at the Fe<sub>B</sub> site. These assignments are supported by the loss of these  $g = 6.2$  and  $6.1$  signals after illumination at cryogenic temperatures, and their

**Table 1. Vibrational Frequencies ( $\text{cm}^{-1}$ ) of Heme  $\{\text{FeNO}\}^7$  Species in the Absence or Presence of Distal Metal Ions**

$\{\text{FeNO}\}^7$ species	$\nu(\text{Fe}-\text{NO})$ ( $\Delta^{15}\text{N}$ ) ( $^*\Delta^{15}\text{N}^{18}\text{O}$ ) <sup>a</sup>	$\nu(\text{N}-\text{O})$ ( $\Delta^{15}\text{N}$ ) ( $^*\Delta^{15}\text{N}^{18}\text{O}$ ) <sup>b</sup>	ref
$\text{Fe}^{\text{II}}\text{-Fe}_B\text{Mb1}(\text{NO})$	577 (−25)	1549 (−22) ( $^*\text{−69}$ )	this work
$\text{Fe}^{\text{II}}\text{-Fe}_B\text{Mb2}(\text{NO})$	578 (−25)	1544 (−25) ( $^*\text{−67}$ )	this work
$\text{Zn}^{\text{II}}\text{-Fe}_B\text{Mb2}(\text{NO})$		1550/1577 (−32) ( $^*\text{−75}$ ) <sup>c</sup>	this work
$\text{Cu}^{\text{I}}\text{-Fe}_B\text{Mb1}(\text{NO})$		1601	this work
$\text{Cu}^{\text{I}}\text{-Fe}_B\text{Mb1}(\text{CO})(\text{NO})$		1629	this work
apo- $\text{Fe}_B\text{Mb1}(\text{NO})$	560 (−24)	1601 (−31)	this work
apo- $\text{Fe}_B\text{Mb2}(\text{NO})$	560 (−24)	nr (−)	this work
swMb(NO)	560 (−28) ( $^*\text{−28}$ )	1613 (−26) ( $^*\text{−68}$ )	25, 36
apo- $\text{Cu}_B\text{Mb}(\text{NO})$	566 ( $^*\text{−20}$ ), 457 ( $^*\text{−11}$ )	1598 ( $^*\text{−35}$ )	19
$\text{Cu}^{\text{I}}\text{-Cu}_B\text{Mb}(\text{NO})$	563 ( $^*\text{−17}$ )	not observed	19
<i>Thermus thermophilus</i> $ba_3(\text{NO})$	539 (−17)	1622 (−32) ( $^*\text{−75}$ )	9, 12
<i>Escherichia coli</i> $bo_3(\text{NO})$	534 ( $^*\text{−17}$ ), 440 ( $^*\text{−13}$ )	1610 (−30) ( $^*\text{−70}$ )	10

<sup>a</sup> From room-temperature RR spectra. <sup>b</sup> From low-temperature FTIR difference spectra except for those of apo- $\text{Cu}_B\text{Mb}(\text{NO})$ . <sup>c</sup> Calculated shifts from the middle of the Fermi doublet.

reappearance after prolonged annealing of these samples in liquid nitrogen (Figure S5 of the Supporting Information).

The nitrosyl complexes that form in apoproteins are stable in the presence of excess NO and allow extended acquisition time for optimal RR spectral characterization. The high-frequency RR spectrum of apo- $\text{Fe}_B\text{Mb1}(\text{NO})$  obtained with 413 nm excitation shows porphyrin skeletal modes  $\nu_4$ ,  $\nu_3$ ,  $\nu_2$ , and  $\nu_{10}$  at 1375, 1502, 1584, and 1636  $\text{cm}^{-1}$ , respectively, as expected for 6cLS heme-NO complexes (Figure 5A).<sup>22,23</sup> Isotope editing with  $^{15}\text{NO}$  of the RR spectra of apo- $\text{Fe}_B\text{Mb1}(\text{NO})$  reveals a very weakly enhanced  $\nu(\text{NO})$  at 1606  $\text{cm}^{-1}$  (Table 1). In the low-frequency RR spectra, a band at 560  $\text{cm}^{-1}$  that downshifts with  $^{15}\text{NO}$  is observed in apo- $\text{Fe}_B\text{Mb1}(\text{NO})$  (Figure 5A) and is assigned to  $\nu(\text{FeNO})$ , as previously reported in wild-type swMb and  $\text{Cu}_B\text{Mb}$ .<sup>19,23</sup> Similar RR data were obtained with apo- $\text{Fe}_B\text{Mb2}(\text{NO})$  (Figure S6A of the Supporting Information).

Because the  $\text{Fe}^{\text{II}}\text{-Fe}_B\text{Mb1}(\text{NO})$  and  $\text{Fe}^{\text{II}}\text{-Fe}_B\text{Mb2}(\text{NO})$  complexes are not stable in the presence of excess NO and when prepared using  $\leq 1$  equiv of NO, the Raman laser probe promotes the dynamic buildup of a significant population of heme iron(II) species via efficient photolysis of 6cLS heme  $\{\text{FeNO}\}^7$  species and slow nongeminate rebinding at low NO concentrations. Indeed, despite low laser power ( $\sim 0.05$  mW) and sample spinning, the high-frequency RR spectrum of  $\text{Fe}^{\text{II}}\text{-Fe}_B\text{Mb1}(\text{NO})$  shows two prominent bands for the oxidation-state marker band  $\nu_4$ , one at 1353  $\text{cm}^{-1}$  that increases with laser power and is also observed in the RR spectrum of reduced  $\text{Fe}^{\text{II}}\text{-Fe}_B\text{Mb1}$  and one at 1375  $\text{cm}^{-1}$  that corresponds to the heme  $\{\text{FeNO}\}^7$  complex (Figure 5B). A difference spectrum can be computed to isolate the components of the nitrosyl complex from the raw data. It reveals porphyrin skeletal modes  $\nu_4$ ,  $\nu_3$ ,  $\nu_2$ , and  $\nu_{10}$  at 1375, 1503, 1583, and 1638  $\text{cm}^{-1}$ , respectively, that are characteristic of a 6cLS heme-nitrosyl species and very similar to those observed with apo- $\text{Fe}_B\text{Mb1}(\text{NO})$  (Figure 5B). While  $\nu(\text{NO})$  values could not be extracted from the RR spectra of  $\text{Fe}^{\text{II}}\text{-Fe}_B\text{Mb1}(\text{NO})$  or  $\text{Fe}^{\text{II}}\text{-Fe}_B\text{Mb2}(\text{NO})$ , an  $^{15}\text{NO}$  isotope sensitive mode at 577  $\text{cm}^{-1}$ , 17  $\text{cm}^{-1}$  higher than in apo- $\text{Fe}_B\text{Mb1}(\text{NO})$ , is assigned to a  $\nu(\text{FeNO})$  vibration from the heme  $\{\text{FeNO}\}^7$  species (Figure 5B). Similar RR data were obtained with  $\text{Fe}^{\text{II}}\text{-Fe}_B\text{Mb2}(\text{NO})$  (Table 1 and Figure S6B of the Supporting Information).

**Low-Temperature Photolysis of the Heme-NO Complexes.** As observed previously with  $ba_3(\text{NO})$  and  $bo_3(\text{NO})$ ,

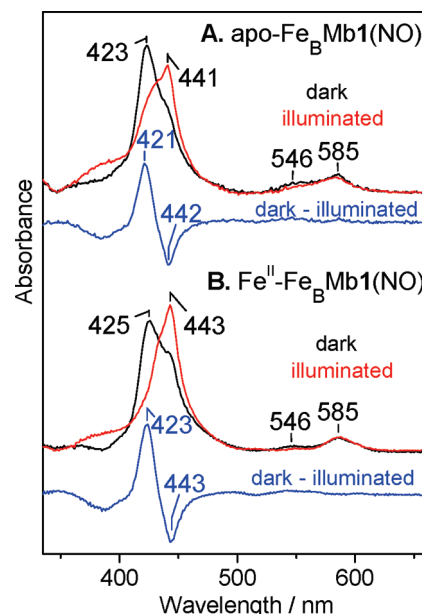


**Figure 6.** UV-vis spectra of apo- $\text{Fe}_B\text{Mb1}(\text{NO})$  (A) and  $\text{Fe}^{\text{II}}\text{-Fe}_B\text{Mb1}(\text{NO})$  (B) at 10 K: dark (black), illuminated (red), and dark minus illuminated difference (blue) spectra. Shoulders at 443 nm in the dark spectra suggest incomplete heme NO occupancy with  $\leq 1$  equiv NO additions.

low-temperature FTIR photolysis experiments were conducted to isolate  $\nu(\text{NO})$  vibrations of metal-nitrosyl complexes in “dark” minus “illuminated” FTIR difference spectra.<sup>9,10</sup> While detection of these modes by RR spectroscopy is hampered by poor enhancement of  $\nu(\text{NO})$  modes (vide supra), the FTIR photolysis approach has been shown to be a sensitive probe of dinuclear heme-copper active sites as well as heme–nonheme diiron sites.<sup>10,24</sup>

The UV-vis spectra of apo- and  $\text{Cu}^{\text{I}}\text{-Fe}_B\text{Mb1}(\text{NO})$  recorded at 10 K show Soret bands at 423 nm that are slightly red-shifted from those observed at room temperature but remain consistent with the assignment of 6cLS heme  $\{\text{FeNO}\}^7$  complexes (Figure 6A). Illumination with a 300 W arc lamp for a few minutes generates a new Soret absorption near 441 nm, characteristic of 5cHS heme iron(II) species, which again are red-shifted by a few

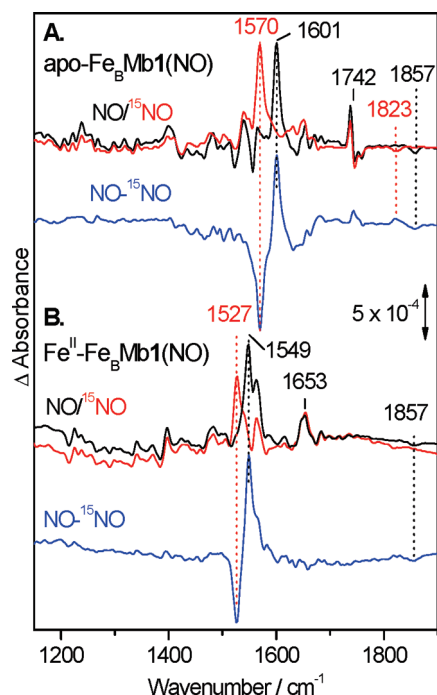


**Figure 7.** FTIR difference spectra (dark minus illuminated) of apo-Fe<sub>B</sub>Mb1(NO) (A) and Fe<sup>II</sup>-Fe<sub>B</sub>Mb1(NO) (B) at 10 K: NO (black), <sup>15</sup>NO (red), and NO minus <sup>15</sup>NO difference spectra (blue).

nanometers from absorption maxima observed in the reduced proteins at room temperature. Dark minus illuminated UV–vis difference spectra reveal differential signals centered near 430 nm that are nearly identical in apo- and Cu<sup>I</sup>-Fe<sub>B</sub>Mb1(NO) and that suggest high photodissociation efficiency (>60%) (Figure 6A and Figure S7 of the Supporting Information). Rebinding of photolyzed NO to the heme requires that the sample temperature be increased to 60 K, which is 20 K higher than for swMb.<sup>25</sup>

The 10 K UV–vis spectrum of Fe<sup>II</sup>-Fe<sub>B</sub>Mb1(NO) shows a Soret band at 425 nm, which is red-shifted by 2 nm compared to that of apo-Fe<sub>B</sub>Mb1(NO), and consistent with a 6cLS heme {FeNO}<sup>7</sup> complex (Figure 6B). Similar to apo-Fe<sub>B</sub>Mb1(NO), this sample shows high photodissociation efficiency with the appearance of a new Soret absorption at 443 nm that matches that of the 5cHS heme iron(II) species observed in reduced Fe<sup>II</sup>-Fe<sub>B</sub>Mb1 at 10 K (data not shown). Equivalent low-temperature UV–vis data were obtained with Fe<sup>II</sup>-Fe<sub>B</sub>Mb2(NO) (data not shown). Complete rebinding of the photolyzed NO to the heme in Fe<sup>II</sup>-Fe<sub>B</sub>Mb1(NO) and Fe<sup>II</sup>-Fe<sub>B</sub>Mb2(NO) occurs quickly only above 110 K, which is at least 50 K higher than in apo-Fe<sub>B</sub>Mb1(NO), suggesting a greater thermodynamic barrier for NO rebinding in presence of Fe<sup>II</sup> at the Fe<sub>B</sub> site.

As observed previously at room temperature, the low-temperature UV–vis spectrum of Zn<sup>II</sup>-Fe<sub>B</sub>Mb2(NO) reveals a broad Soret absorption with multiple shoulders indicative of a mixture of species. Despite this mixture, the differential signal observed in the dark minus illuminated UV–vis difference spectrum is qualitatively the same as that of Fe<sup>II</sup>-Fe<sub>B</sub>Mb2(NO) (Figure S8 of the Supporting Information) as only 6cLS heme {FeNO}<sup>7</sup> species are readily photolyzed under the conditions used here.<sup>9</sup> Equivalent experiments with Zn<sup>II</sup>-Fe<sub>B</sub>Mb1(NO) revealed only a marginal differential signal in the Soret region (data not shown) in support of the low content of 6cLS {FeNO}<sup>7</sup>

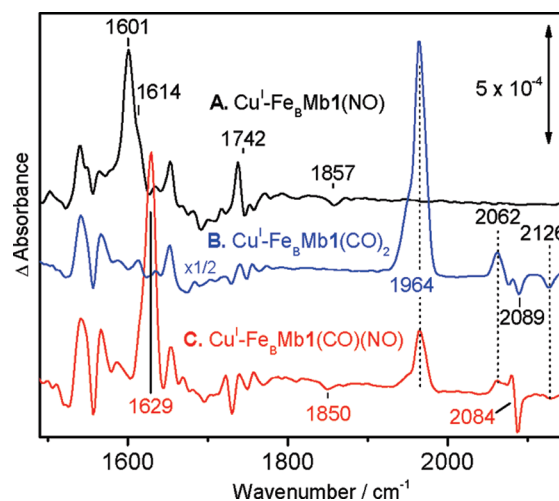


**Figure 8.** FTIR difference spectra (dark minus illuminated) of Cu<sup>I</sup>-Fe<sub>B</sub>Mb1(NO) (A), Cu<sup>I</sup>-Fe<sub>B</sub>Mb1(CO)<sub>2</sub> (B), and Cu<sup>I</sup>-Fe<sub>B</sub>Mb1(CO)(NO) (C) at 10 K.

species observed in these samples by EPR spectroscopy (see above). The temperature dependence of NO rebinding after photolysis in Zn<sup>II</sup>-Fe<sub>B</sub>Mb2(NO) is equivalent to that of Fe<sup>II</sup>-Fe<sub>B</sub>Mb1(NO) and Fe<sup>II</sup>-Fe<sub>B</sub>Mb2(NO).

The dark minus illuminated FTIR difference spectra of apo-Fe<sub>B</sub>Mb1(NO) obtained at 10 K isolate a positive band at 1601 cm<sup>-1</sup> that downshifts to 1570 (−31) cm<sup>-1</sup> with <sup>15</sup>NO and is assigned to ν(NO) of the heme-NO complex (Figure 7A). This frequency is a close match to the ν(NO) observed in the RR spectra. The difference spectra also reveal a negative band at 1857 cm<sup>-1</sup> that downshifts to 1823 (−34) cm<sup>-1</sup> with <sup>15</sup>NO and that we assign to a ν(NO) from the photolyzed NO group docked in a proteinaceous pocket. Equivalent dissociated ν(NO) features have been observed for the nitrosyl complexes of myoglobin and some HCOs.<sup>10,25</sup> In addition to these FTIR bands related to the NO group, the dark minus illuminated FTIR difference spectra include weaker signals between 1200 and 1750 cm<sup>-1</sup> that cancel out in the NO isotope-edited difference spectra and are thus assigned to perturbations of amide and porphyrin vibrational modes. A relatively intense differential signal centered at 1742 cm<sup>-1</sup> is assigned to a C=O stretching mode of a carboxylic acid, possibly E68 because this residue may interact with the bound NO and could report perturbations upon NO dissociation.

The FTIR difference spectrum of Cu<sup>I</sup>-Fe<sub>B</sub>Mb1(NO) is nearly identical to that of apo-Fe<sub>B</sub>Mb1(NO); the difference spectrum isolates ν(NO) features from the heme {FeNO}<sup>7</sup> complex and free NO docked in the distal pocket at 1601 and 1857 cm<sup>-1</sup>, respectively (Figure 8A). The 1742 cm<sup>-1</sup> differential signal observed in apo-Fe<sub>B</sub>Mb1(NO) is also conserved and may reflect the lack of affinity of Cu<sup>I</sup> for carboxylate ligands. In view of these similarities between Cu<sup>I</sup>-Fe<sub>B</sub>Mb1 and apo-Fe<sub>B</sub>Mb1, a concern was that Cu<sup>I</sup> might not be retained at the Fe<sub>B</sub> site, but this interpretation of the data is ruled out by experiments with CO. Specifically, exposing fully reduced Cu<sup>I</sup>-Fe<sub>B</sub>Mb1 to excess CO results in a full conversion of the broad 433 nm Soret absorption of ferrous heme to a sharp Soret band at 422 nm (Figure S9 of the Supporting Information). Low-temperature FTIR spectra of these samples reveal the concomitant presence of ν(CO)<sub>heme</sub> and ν(CO)<sub>Cu</sub> at 1950/1964 and 2068/2083 cm<sup>-1</sup>, respectively



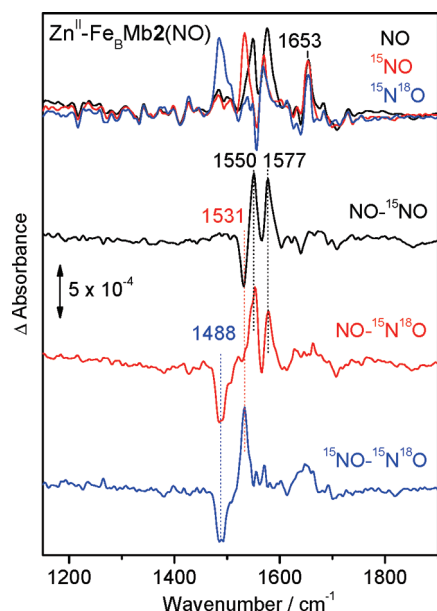


**Figure 9.** FTIR difference spectra (dark minus illuminated) of  $\text{Zn}^{\text{II}}\text{-Fe}_B\text{Mb2}(\text{NO})$  at 10 K: NO (black),  $^{15}\text{NO}$  (red),  $^{15}\text{N}^{18}\text{O}$  (blue), and isotope difference spectra of NO minus  $^{15}\text{NO}$  (black), NO minus  $^{15}\text{N}^{18}\text{O}$  (red), and  $^{15}\text{NO}$  minus  $^{15}\text{N}^{18}\text{O}$  (blue).

(Figure S10 of the Supporting Information). These data suggest that the heme-copper dinuclear site in  $\text{Fe}_B\text{Mb1}$  is capable of accommodating two CO molecules to form a  $\text{Cu}^{\text{I}}\text{-Fe}_B\text{Mb1}(\text{CO})_2$  ternary complex. The two sets of  $\nu(\text{CO})_{\text{heme}}$  and  $\nu(\text{CO})_{\text{Cu}}$  frequencies are likely to correspond to two distinct  $\text{Cu}^{\text{I}}\text{-Fe}_B\text{Mb1}(\text{CO})_2$  conformers and are reminiscent of the  $\alpha/\beta$  conformers observed in some HCOs such as those from *Rhodobacter sphaeroides aa3*.<sup>26</sup> Although a dicarbonyl complex has been shown to form at the diiron site of one NOR, the  $\text{qCu}_A\text{NOR}$  from *Bacillus azotoformans*,<sup>24</sup> it has not been observed in HCOs.

To confirm the presence of  $\text{Cu}^{\text{I}}$  at the  $\text{Fe}_B$  site in  $\text{Fe}_B\text{Mb1}$  after addition of 1 equiv of NO, we also prepared the [heme-NO·OC-Cu] ternary complex. An equivalent ternary complex was characterized earlier in *bo3*.<sup>10</sup> The FTIR dark spectrum of  $\text{Cu}^{\text{I}}\text{-Fe}_B\text{Mb1}(\text{CO})(\text{NO})$  shows absorption at 2071 and 2083  $\text{cm}^{-1}$ , consistent with  $\nu(\text{CO})_{\text{Cu}}$  frequencies, while the heme iron is predominantly complexed by NO (Figure S11 of the Supporting Information). The FTIR photolysis difference spectra of  $\text{Cu}^{\text{I}}\text{-Fe}_B\text{Mb1}(\text{CO})(\text{NO})$  show a  $\nu(\text{NO})_{\text{heme}}$  at 1629  $\text{cm}^{-1}$  that is upshifted by 28  $\text{cm}^{-1}$  in the presence of the Cu-carbonyl (Figure 8C). The NO dissociation induces new perturbations in the  $\nu(\text{CO})_{\text{Cu}}$  region at 2084  $\text{cm}^{-1}$  (Figure 8C). The absence of  $\nu(\text{NO})$  near 1601  $\text{cm}^{-1}$ , as in apo- $\text{Fe}_B\text{Mb1}(\text{NO})$  or  $\text{Cu}^{\text{I}}\text{-Fe}_B\text{Mb1}(\text{NO})$ , suggests that the formation of the [heme-NO·OC-Cu] ternary complex is stoichiometric. The presence of  $\text{Cu}^{\text{I}}$  or  $\text{Cu}^{\text{I}}\text{-CO}$  at the  $\text{Fe}_B$  site has no effect on the rebinding temperature of the heme  $\{\text{FeNO}\}^7$  complexes in  $\text{Cu}^{\text{I}}\text{-Fe}_B\text{Mb1}(\text{NO})$  and  $\text{Cu}^{\text{I}}\text{-Fe}_B\text{Mb1}(\text{CO})(\text{NO})$  that occur after annealing to 60 K as in apo- $\text{Fe}_B\text{Mb1}(\text{NO})$ .

Although binding of  $\text{Fe}^{\text{II}}$  to the  $\text{Fe}_B$  site does not significantly affect the electronic absorption spectrum of the heme  $\{\text{FeNO}\}^7$  species in  $\text{Fe}_B\text{Mbs}$  (Figure 2B and Figure S3 of the Supporting Information), it leads to a 50  $\text{cm}^{-1}$  downshift of the  $\nu(\text{NO})_{\text{heme}}$  mode. Specifically,  $\nu(\text{NO})_{\text{heme}}$  is observed as a positive band at 1549  $\text{cm}^{-1}$  in the FTIR difference spectra that downshifts to

1527 ( $-22$ )  $\text{cm}^{-1}$  with  $^{15}\text{NO}$  (Figure 7B and Table 1). Weaker differential signals between 1200 and 1700  $\text{cm}^{-1}$  cancel out in the NO isotope-edited difference spectra and are assigned to perturbations of amide and porphyrin vibrational modes. The strong differential signal at 1742  $\text{cm}^{-1}$  observed in the FTIR difference spectra of apo- $\text{Fe}_B\text{Mb1}(\text{NO})$  and assigned to the C=O stretch of E68 is absent from the difference spectra of  $\text{Fe}^{\text{II}}\text{-Fe}_B\text{Mb1}(\text{NO})$ , presumably as E68 is recruited for coordination of  $\text{Fe}^{\text{II}}$  at the  $\text{Fe}_B$  site.<sup>15,16</sup> Reproducible detection of a negative band that could be assigned to free NO docked in a proteinaceous pocket was not achieved with  $\text{Fe}^{\text{II}}\text{-Fe}_B\text{Mb1}(\text{NO})$  samples and may reflect heterogeneous broadening from multiple NO-docking sites in  $\text{Fe}^{\text{II}}\text{-Fe}_B\text{Mb1}$  compared to apo- $\text{Fe}_B\text{Mb1}$ .

Introducing an additional glutamate residue into  $\text{Fe}_B\text{Mb2}$  further lowers the  $\nu(\text{NO})_{\text{heme}}$  in  $\text{Fe}^{\text{II}}\text{-Fe}_B\text{Mb2}(\text{NO})$  by 5  $\text{cm}^{-1}$ . The 10 K dark minus illuminated FTIR difference spectrum of the  $\text{Fe}^{\text{II}}\text{-Fe}_B\text{Mb2}(\text{NO})$  complex exhibits a  $\nu(\text{NO})_{\text{heme}}$  at 1544  $\text{cm}^{-1}$  that downshifts to 1519 ( $-25$ ) and 1477 ( $-67$ )  $\text{cm}^{-1}$  with  $^{15}\text{NO}$  and  $^{15}\text{N}^{18}\text{O}$ , respectively (Figure S11 of the Supporting Information). A broad and weak negative band at 1850  $\text{cm}^{-1}$  that downshifts to 1819 ( $-31$ ) and 1769 ( $-81$ )  $\text{cm}^{-1}$  with  $^{15}\text{NO}$  and  $^{15}\text{N}^{18}\text{O}$ , respectively, is assigned to the  $\nu(\text{NO})_{\text{free}}$  from NO docked in proteinaceous pocket(s).

To investigate the effect of metal ion composition at the  $\text{Fe}_B$  site, we performed FTIR photolysis experiments also with the  $\text{Zn}^{\text{II}}\text{-Fe}_B\text{Mb2}(\text{NO})$  complex. The FTIR difference spectra of  $\text{Zn}^{\text{II}}\text{-Fe}_B\text{Mb2}(\text{NO})$  show a doublet at 1550/1577  $\text{cm}^{-1}$  that downshifts as a singlet at 1531 and 1488  $\text{cm}^{-1}$  with  $^{15}\text{NO}$  and  $^{15}\text{N}^{18}\text{O}$ , respectively (Figure 9 and Table 1). Thus, the 1550/1577  $\text{cm}^{-1}$  doublet is assigned to a Fermi coupling of the  $\nu(^{14}\text{NO})$  mode in  $\text{Zn}^{\text{II}}\text{-Fe}_B\text{Mb2}(\text{NO})$ . As with  $\text{Fe}^{\text{II}}\text{-Fe}_B\text{Mb2}(\text{NO})$ , the  $\nu(\text{NO})$  of free NO is not detected in a reproducible fashion in  $\text{Zn}^{\text{II}}\text{-Fe}_B\text{Mb2}(\text{NO})$ .

## DISCUSSION

Stoichiometric additions of NO to fully reduced  $\text{Fe}^{\text{II}}\text{-Fe}_B\text{Mb1}$  and  $\text{Fe}^{\text{II}}\text{-Fe}_B\text{Mb2}$  result in the formation of stable heme-NO complexes, suggesting that the 5cHS ferrous heme irons exhibit higher affinity for NO than the nonheme  $\text{Fe}^{\text{II}}$  sites. While the UV-vis and high-frequency RR spectra of  $\text{Fe}^{\text{II}}\text{-Fe}_B\text{Mb}(\text{NO})$  are nearly identical to those of apo- $\text{Fe}_B\text{Mb}(\text{NO})$  and characteristic of 6cLS heme  $\{\text{FeNO}\}^7$  species, the  $\text{Fe}^{\text{II}}\text{-Fe}_B\text{Mb}(\text{NO})$  complexes exhibit unusual Fe-N-O vibrational frequencies. Typically, 6cLS heme  $\{\text{FeNO}\}^7$  species can display two low-frequency RR modes sensitive to NO isotope labeling: one near 450  $\text{cm}^{-1}$  and another near 560  $\text{cm}^{-1}$ . Here, only the latter signal is observed with significant enhancement, and it occurs at 577 and 578  $\text{cm}^{-1}$  in  $\text{Fe}^{\text{II}}\text{-Fe}_B\text{Mb1}(\text{NO})$  and  $\text{Fe}^{\text{II}}\text{-Fe}_B\text{Mb2}(\text{NO})$ , respectively, i.e., 17–18  $\text{cm}^{-1}$  higher than in the apoproteins. Assignments of these bands as Fe-NO stretching and Fe-N-O bending modes has been a recurring source of controversy,<sup>22,23,27</sup> and although combined analyses of RR and nuclear resonance vibrational spectroscopy (NRVS) data and density function theory (DFT) calculations have made a convincing case for assigning the vibration near 560  $\text{cm}^{-1}$  to the bending mode and the lower-frequency band as a mixed stretching and bending mode,<sup>28,29</sup> interpreting observed frequencies in terms of bond strength and/or bond geometry remains arduous. In contrast, N-O stretches from iron-nitrosyl species behave as isolated modes, and accordingly, the fact that the  $\nu(\text{NO})$  features of  $\text{Fe}^{\text{II}}\text{-Fe}_B\text{Mb1}(\text{NO})$  and  $\text{Fe}^{\text{II}}\text{-Fe}_B\text{Mb2}(\text{NO})$  are  $\sim 50$   $\text{cm}^{-1}$  lower

than in all heme-nitrosyl complexes reported so far is highly significant.<sup>30,31</sup> Taken together with the results of metal ion substitution at the Fe<sub>B</sub> site, these vibrational data suggest a bent FeNO geometry and an Fe(III)-NO<sup>-</sup> resonance structure with an increased level of iron d $\pi$  to NO  $\pi^*$  backbonding<sup>30,32,33</sup> with stabilization via electrostatic interaction with the Fe<sup>II</sup> ion at the Fe<sub>B</sub> site.

The data obtained with Zn<sup>II</sup>-Fe<sub>B</sub>Mb2(NO) support this assignment of the Fe<sub>B</sub> site perturbation on the heme {FeNO}<sup>7</sup> species as being primarily electrostatic, because the  $\nu$ (NO) mode in Zn<sup>II</sup>-Fe<sub>B</sub>Mb2(NO) is observed only  $\sim 10$  cm<sup>-1</sup> higher than in Fe<sup>II</sup>-Fe<sub>B</sub>Mb2(NO). This small shift in  $\nu$ (NO) frequencies may reflect a difference in the distance between the heme {FeNO}<sup>7</sup> unit and the nonheme divalent ion and/or difference in the extent of charge neutralization induced by the carboxylate group of E68 on the divalent ion. Crystal structures, which are available for air-oxidized Zn<sup>II</sup>-Fe<sub>B</sub>Mb2 and reduced Fe<sup>II</sup>-Fe<sub>B</sub>Mb2, reveal similar coordination spheres around the divalent nonheme ions, although the distance between the Fe<sub>B</sub> metal ion increases from 4.62 Å in Fe<sup>II</sup>-Fe<sub>B</sub>Mb2 to 4.78 Å in Zn<sup>II</sup>-Fe<sub>B</sub>Mb2 and the carboxylate group of E68 seems to adopt a stronger bidentate coordination with the Zn<sup>II</sup> ion while it appears closer to a  $\mu$ -1,3 bridging geometry between the two iron(II) atoms in Fe<sup>II</sup>-Fe<sub>B</sub>Mb2.<sup>16</sup>

The crystal structure of Cu<sup>II</sup>-loaded air-oxidized Fe<sub>B</sub>Mb2 confirms that Cu<sup>II</sup> ions occupy the Fe<sub>B</sub> site,<sup>16</sup> but a Cu<sup>II</sup>-Fe<sub>B</sub>Mb(NO) complex cannot be formed, presumably because the reduction potential of the Cu<sup>II</sup> is higher than that of the heme iron(II). Cu<sup>I</sup>-Fe<sub>B</sub>Mb(NO), on the other hand, forms readily and shows a  $\nu$ (NO)<sub>heme</sub> mode comparable to that of apo-Fe<sub>B</sub>Mb1-(NO), suggesting that the heme {FeNO}<sup>7</sup> unit does not interact with Cu<sup>I</sup>. While the crystal structure of Cu<sup>II</sup>-Fe<sub>B</sub>Mb indicates that E68 interacts weakly with the Cu<sup>II</sup> ion, this side chain is unlikely to bind to Cu<sup>I</sup>. In fact, a differential signal at 1742 cm<sup>-1</sup> observed in the FTIR photolysis spectra of apo- and Cu<sup>I</sup>-Fe<sub>B</sub>Mb(NO) likely corresponds to  $\nu$ (C=O) of the protonated glutamic acid group of E68. The Cu<sup>I</sup> ion is more likely to coordinate only the three histidine side chains at the Fe<sub>B</sub> site. This coordination geometry may also result in a greater distance between the heme iron and the copper ion and allow the Cu<sup>I</sup> ion to bind CO in the presence of a second exogenous ligand at the heme iron.

Interaction between the heme {FeNO}<sup>7</sup> species and the nonheme Fe<sup>II</sup> is also evidenced by the impact of metal occupancy at the Fe<sub>B</sub> site on the detection of the  $g \sim 2$  signal observed in apo-Fe<sub>B</sub>Mb(NO). While the incorporation of diamagnetic Cu<sup>I</sup> and Zn<sup>II</sup> affects only the characteristics of the  $g \sim 2$  signal from the heme {FeNO}<sup>7</sup> species, the addition of Fe<sup>II</sup> completely banishes the detection of this EPR signal. Exchange coupling between an  $S = 1/2$  heme {FeNO}<sup>7</sup> and an  $S = 2$  high-spin Fe<sub>B</sub><sup>II</sup> is anticipated to produce a noninteger overall spin that can be observed by EPR. Accordingly, new  $g = 6.2$  and  $6.1$  resonances that can be observed only below 30 K in Fe<sup>II</sup>-Fe<sub>B</sub>Mb1(NO) and Fe<sup>II</sup>-Fe<sub>B</sub>Mb2(NO), respectively, are likely to reflect these paramagnetic clusters. Further investigation will be required to fully define the magnetic properties of these complexes, but the photosensitive character of these EPR features supports these preliminary assignments (Supporting Information).

Our data identify a 6cLS heme {FeNO}<sup>7</sup> weakly interacting with the Fe<sub>B</sub><sup>II</sup> site to produce a partial nitroxyl anion as the first complex formed by exposure of reduced Fe<sub>B</sub>Mb models to NO. This structural model is consistent with DFT analyses of the NO reduction reaction at heme–nonheme diiron sites that predict the presence of a stabilizing interaction between the negatively

charged nitroxyl anion and Fe<sub>B</sub><sup>II</sup>.<sup>14</sup> A similar intermediate complex was proposed to form in flow-flash experiments with cNOR(CO) exposed to NO, where UV–vis spectra suggest that a first NO reacts with high-spin heme  $b_3$  within 2  $\mu$ s to form a six-coordinate heme-nitrosyl complex.<sup>34</sup>

Subsequent steps in the formation of this initial [6cLS heme {FeNO}<sup>7</sup>·nonheme Fe<sub>B</sub><sup>II</sup>] complex remain obscure. Rapid-freeze-quench EPR experiments by Shiro and co-workers suggest that dissociation of the proximal His ligand from the heme  $b_3$  to form a five-coordinate heme-nitrosyl complex and binding of a second NO to the Fe<sub>B</sub> center occur on a submillisecond time scale to form a [5cLS heme {FeNO}<sup>7</sup>·nonheme {FeNO}<sup>7</sup>] ternary complex.<sup>35</sup> In contrast, a DFT analysis by Siegbahn et al. predicted a direct attack of a second NO on the heme-nitroxyl complex coupled with electron transfer from Fe<sub>B</sub><sup>II</sup> to form a heme iron(III)-bound hyponitrite dianion intermediate.<sup>14</sup> Preliminary experiments monitoring the reaction of NO with Fe<sup>II</sup>-Fe<sub>B</sub>Mb(NO) complexes suggest that both 5cLS and 6cLS heme {FeNO}<sup>7</sup> species as well as nonheme {FeNO}<sup>7</sup> are forming in these models. Stopped-flow and rapid-freeze-quench experiments, in parallel with vibrational analyses, to characterize the products of Fe<sub>B</sub>Mb(NO) complexes exposed NO are being conducted.

## ■ ASSOCIATED CONTENT

**S Supporting Information.** Room-temperature UV–vis absorption and RR spectra of reduced apo-, Fe<sup>II</sup>-, Zn<sup>II</sup>-, and Cu<sup>I</sup>-Fe<sub>B</sub>Mb2 before and after addition of 1 equiv of NO; EPR spectra of apo-, Fe<sup>II</sup>-, Zn<sup>II</sup>-, and Cu<sup>I</sup>-Fe<sub>B</sub>Mb(NO) at 30 and 4.2 K; low-temperature UV–vis spectra of Zn<sup>II</sup>- and Cu<sup>I</sup>-Fe<sub>B</sub>Mb2-(NO); room-temperature UV–vis spectra of Cu<sup>I</sup>-Fe<sub>B</sub>Mb2-(CO)<sub>2</sub> and Cu<sup>I</sup>-Fe<sub>B</sub>Mb2(CO)(NO); and low-temperature FTIR spectra of Cu<sup>I</sup>-Fe<sub>B</sub>Mb2(CO)<sub>2</sub>, Cu<sup>I</sup>-Fe<sub>B</sub>Mb2(CO)(NO), and Fe<sup>II</sup>-Fe<sub>B</sub>Mb2(NO). This material is available free of charge via the Internet at <http://pubs.acs.org>.

## ■ AUTHOR INFORMATION

### Corresponding Author

\*Oregon Health and Science University, 20000 NW Walker Rd., Beaverton, OR 97006. Telephone: (503) 748-1673. Fax: (503) 748-1464. E-mail: [ploccoz@ebs.ogi.edu](mailto:ploccoz@ebs.ogi.edu).

### Funding Sources

This work was supported by Grants GM74785 (P.M.-L.) and GM06221 (Y.L.) from the National Institutes of Health and a Vertex pharmaceutical scholarship (T.H.).

## ■ ABBREVIATIONS

NOR, nitric oxide reductase; HCO, heme-copper oxidase; swMb, sperm whale myoglobin; Fe<sub>B</sub>Mb1, swMb L29H/F43H/V68E variant; Fe<sub>B</sub>Mb2, swMb L29H/F43H/V68E/I107E variant; Cu<sub>B</sub>Mb, swMb L29H/F43H variant; RR, resonance Raman; EPR, electron paramagnetic resonance; FTIR, Fourier transform infrared; 6C and 5C, six-coordinate and five-coordinate, respectively; HS and LS, high-spin and low-spin, respectively.

## ■ REFERENCES

- (1) Wasser, I. M., de Vries, S., Moënné-Loccoz, P., Schroder, I., and Karlin, K. D. (2002) Nitric oxide in biological denitrification: Fe/Cu metalloenzyme and metal complex NO<sub>x</sub> redox chemistry. *Chem. Rev.* 102, 1201–1234.



- (2) Zumft, W. G. (2005) Nitric oxide reductases of prokaryotes with emphasis on the respiratory, heme-copper oxidase type. *J. Inorg. Biochem.* 99, 194–215.
- (3) Moënné-Loccoz, P. (2007) Spectroscopic characterization of heme iron-nitrosyl species and their role in NO reductase mechanisms in diiron proteins. *Nat. Prod. Rep.* 24, 610–620.
- (4) Barraud, N., Hassett, D. J., Hwang, S. H., Rice, S. A., Kjelleberg, S., and Webb, J. S. (2006) Involvement of nitric oxide in biofilm dispersal of *Pseudomonas aeruginosa*. *J. Bacteriol.* 188, 7344–7353.
- (5) Stevanin, T. M., Laver, J. R., Poole, R. K., Moir, J. W., and Read, R. C. (2007) Metabolism of nitric oxide by *Neisseria meningitidis* modifies release of NO-regulated cytokines and chemokines by human macrophages. *Microbes Infect.* 9, 981–987.
- (6) Hino, T., Matsumoto, Y., Nagano, S., Sugimoto, H., Fukumori, Y., Murata, T., Iwata, S., and Shiro, Y. (2010) Structural basis of biological N<sub>2</sub>O generation by bacterial nitric oxide reductase. *Science* 330, 1666–1670.
- (7) Butler, C., Forte, E., Maria Scandurra, F., Arese, M., Giuffrè, A., Greenwood, C., and Sarti, P. (2002) Cytochrome *bo*<sub>3</sub> from *Escherichia coli*: The binding and turnover of nitric oxide. *Biochem. Biophys. Res. Commun.* 296, 1272–1278.
- (8) Fujiwara, T., and Fukumori, Y. (1996) Cytochrome *cb*-type nitric oxide reductase with cytochrome *c* oxidase activity from *Paracoccus denitrificans* ATCC 35512. *J. Bacteriol.* 178, 1866–1871.
- (9) Hayashi, T., Lin, J. J., Chen, Y., Fee, J. A., and Moënné-Loccoz, P. (2007) Fourier transform infrared characterization of a Cu<sub>B</sub>-nitrosyl complex in cytochrome *ba*<sub>3</sub> from *Thermus thermophilus*: relevance to NO reductase activity in heme-copper terminal oxidases. *J. Am. Chem. Soc.* 129, 14952–14958.
- (10) Hayashi, T., Lin, M. T., Ganesan, K., Chen, Y., Fee, J. A., Gennis, R. B., and Moënné-Loccoz, P. (2009) Accommodation of two diatomic molecules in cytochrome *bo*<sub>3</sub>: Insights into NO reductase activity in terminal oxidases. *Biochemistry* 48, 883–890.
- (11) Ohta, T., Kitagawa, T., and Varotsis, C. (2006) Characterization of a bimetallic-bridging intermediate in the reduction of NO to N<sub>2</sub>O: A density functional theory study. *Inorg. Chem.* 45, 3187–3190.
- (12) Pinakoulaki, E., Ohta, T., Soulimane, T., Kitagawa, T., and Varotsis, C. (2005) Detection of the His-heme Fe<sup>2+</sup>-NO species in the reduction of NO to N<sub>2</sub>O by *ba*<sub>3</sub>-oxidase from *Thermus thermophilus*. *J. Am. Chem. Soc.* 127, 15161–15167.
- (13) Blomberg, L. M., Blomberg, M. R., and Siegbahn, P. E. (2006) A theoretical study on nitric oxide reductase activity in a *ba*<sub>3</sub>-type heme-copper oxidase. *Biochim. Biophys. Acta* 1757, 31–46.
- (14) Blomberg, L. M., Blomberg, M. R., and Siegbahn, P. E. (2006) Reduction of nitric oxide in bacterial nitric oxide reductase: A theoretical model study. *Biochim. Biophys. Acta* 1757, 240–252.
- (15) Yeung, N., Lin, Y. W., Gao, Y. G., Zhao, X., Russell, B. S., Lei, L., Miner, K. D., Robinson, H., and Lu, Y. (2009) Rational design of a structural and functional nitric oxide reductase. *Nature* 462, 1079–1082.
- (16) Lin, Y. W., Yeung, N., Gao, Y. G., Miner, K. D., Tian, S., Robinson, H., and Lu, Y. (2010) Roles of glutamates and metal ions in a rationally designed nitric oxide reductase based on myoglobin. *Proc. Natl. Acad. Sci. U.S.A.* 107, 8581–8586.
- (17) Kitagawa, T., Nagai, K., and Tsubaki, M. (1979) Assignment of the Fe-Ne (His F8) stretching band in the resonance Raman spectra of deoxy myoglobin. *FEBS Lett.* 104, 376–378.
- (18) Argade, P. V., Sassaroli, M., Rousseau, D. L., Inubushi, T., Ikeda-Saito, M., and Lapidot, A. (1984) Confirmation of the assignment of the iron-histidine stretching mode in myoglobin. *J. Am. Chem. Soc.* 106, 6593–6596.
- (19) Lu, C., Zhao, X., Lu, Y., Rousseau, D. L., and Yeh, S. R. (2010) Role of copper ion in regulating ligand binding in a myoglobin-based cytochrome *c* oxidase model. *J. Am. Chem. Soc.* 132, 1598–1605.
- (20) Bolard, J., and Garnier, A. (1972) Circular dichroism studies of myoglobin and cytochrome *c* derivatives. *Biochim. Biophys. Acta* 263, 535–549.
- (21) Szabo, A., and Perutz, M. F. (1976) Equilibrium between six- and five-coordinated hemes in nitrosylhemoglobin: Interpretation of electron spin resonance spectra. *Biochemistry* 15, 4427–4428.
- (22) Benko, B., and Yu, N. T. (1983) Resonance Raman studies of nitric oxide binding to ferric and ferrous hemoproteins: Detection of Fe(III)-NO stretching, Fe(III)-N-O bending, and Fe(II)-N-O bending vibrations. *Proc. Natl. Acad. Sci. U.S.A.* 80, 7042–7046.
- (23) Tsubaki, M., and Yu, N. T. (1982) Resonance Raman investigation of nitric oxide bonding in nitrosylhemoglobin A and -myoglobin: Detection of bound N-O stretching and Fe-NO stretching vibrations from the hexacoordinated NO-heme complex. *Biochemistry* 21, 1140–1144.
- (24) Lu, S., Suharti, de Vries, S., and Moënné-Loccoz, P. (2004) Two CO molecules can bind concomitantly at the diiron site of NO reductase from *Bacillus azotoformans*. *J. Am. Chem. Soc.* 126, 15332–15333.
- (25) Miller, L. M., Pedraza, A. J., and Chance, M. R. (1997) Identification of conformational substates involved in nitric oxide binding to ferric and ferrous myoglobin through difference Fourier transform infrared spectroscopy (FTIR). *Biochemistry* 36, 12199–12207.
- (26) Alben, J. O., Moh, P. P., Fiamingo, F. G., and Altschuld, R. A. (1981) Cytochrome oxidase *a*<sub>3</sub> heme and copper observed by low-temperature Fourier transform infrared spectroscopy of the CO complex. *Proc. Natl. Acad. Sci. U.S.A.* 78, 234–237.
- (27) Stong, J. D., Burke, J. M., Daly, P., Wright, P., and Spiro, T. G. (1980) Resonance Raman spectra of nitrosyl heme proteins and of porphyrin analogues. *J. Am. Chem. Soc.* 102, 5815–5819.
- (28) Zeng, W., Silvernail, N. J., Wharton, D. C., Georgiev, G. Y., Leu, B. M., Scheidt, W. R., Zhao, J., Sturhahn, W., Alp, E. E., and Sage, J. T. (2005) Direct probe of iron vibrations elucidates NO activation of heme proteins. *J. Am. Chem. Soc.* 127, 11200–11201.
- (29) Lehnert, N., Sage, J. T., Silvernail, N., Scheidt, W. R., Alp, E. E., Sturhahn, W., and Zhao, J. (2010) Oriented single-crystal nuclear resonance vibrational spectroscopy of [Fe(TPP)(MI)(NO)]: Quantitative assessment of the *trans* effect of NO. *Inorg. Chem.* 49, 7197–7215.
- (30) Coyle, C. M., Vogel, K. M., Rush, T. S., III, Kozlowski, P. M., Williams, R., Spiro, T. G., Dou, Y., Ikeda-Saito, M., Olson, J. S., and Zgierski, M. Z. (2003) FeNO structure in distal pocket mutants of myoglobin based on resonance Raman spectroscopy. *Biochemistry* 42, 4896–4903.
- (31) Thomas, M. R., Brown, D., Franzen, S., and Boxer, S. G. (2001) FTIR and resonance Raman studies of nitric oxide binding to H93G cavity mutants of myoglobin. *Biochemistry* 40, 15047–15056.
- (32) Ibrahim, M., Xu, C., and Spiro, T. G. (2006) Differential sensing of protein influences by NO and CO vibrations in heme adducts. *J. Am. Chem. Soc.* 128, 16834–16845.
- (33) Vogel, K. M., Kozlowski, P. M., Zgierski, M. Z., and Spiro, T. G. (1999) Determinants of the FeXO (X = C, N, O) vibrational frequencies in heme adducts from experiment and density function theory. *J. Am. Chem. Soc.* 121, 9915–9921.
- (34) Hendriks, J. H., Jasaitis, A., Saraste, M., and Verkhovsky, M. I. (2002) Proton and electron pathways in the bacterial nitric oxide reductase. *Biochemistry* 41, 2331–2340.
- (35) Kumita, H., Matsuura, K., Hino, T., Takahashi, S., Hori, H., Fukumori, Y., Morishima, I., and Shiro, Y. (2004) NO reduction by nitric-oxide reductase from denitrifying bacterium *Pseudomonas aeruginosa*: Characterization of reaction intermediates that appear in the single turnover cycle. *J. Biol. Chem.* 279, 55247–55254.
- (36) Tomita, T., Hirota, S., Ogura, T., Olson, J. S., and Kitagawa, T. (1999) Resonance Raman investigation of Fe-N-O structure of nitrosylheme in myoglobin and its mutants. *J. Phys. Chem. B* 103, 7044–7054.